LAWRENCE
LIVERMORE
NATIONAL
LABORATORY

LLNL-PROC-761461

The sudden viscous dissipation of compressing turbulence for a two-component fluid

A. Campos, B. Morgan

November 12, 2018

16th International Workshop on the Physics of Compressible Turbulent Mixing
Marseille, France
July 15, 2018 through July 20, 2018

Disclaimer

The sudden viscous dissipation of compressing turbulence for a two-component fluid

A. Campos and B. Morgan
Lawrence Livermore National Laboratory
campos33@llnl.gov

Abstract

Computational simulations of a sudden viscous dissipative mechanism relevant to inertial confinement fusion are carried out for a two-component fluid mixture under compression. The sudden viscous dissipation of turbulent kinetic energy into heat is still observed for this new case. The evolution of the mass-fraction variance as the fluid is compressed at various rates is also computed, and a decay of the mass-fraction fluctuations due to the viscous dissipative mechanism is demonstrated.

I. Introduction

Turbulence can have a substantial effect in high-energy-density experiments (see, for example [1, 2]). In particular, a transition to turbulent mixing in inertial confinement fusion (ICF) has the potential to increase unwanted mix between hot and cold materials, thus deteriorating the efficacy of an ICF implosion. However, previous work [3] has suggested that an unexpected dissipative mechanism of turbulence could be exploited to enhance conditions for ignition during an ICF implosion. Through computational simulations that used a plasma scaling for viscosity ($\mu \sim T^{5/2}$) rather than a fluid scaling ($\mu \sim T^{3/4}$), Davidovits & Fisch [3] demonstrated that, as a turbulent flow is compressed, the effect of viscosity eventually dominates and a sudden and rapid viscous dissipation eliminates the turbulent kinetic energy (TKE) in the system. This dissipated TKE would thus lead to increased internal energies and temperatures, which would improve conditions for ignition.

Numerous additional studies have further investigated the sudden dissipative mechanism [4, 5, 6, 7]. In particular, [8] extended previous work that had so far been confined to the zero-Mach-limit by instead solving compressible Navier-Stokes equations for turbulence in the finite-Mach-number regime. This approach allows for the explicit representation of the self-consistent transfer of energy between the TKE and the internal energy, and the subsequent effect that the altered viscosity has on the original TKE viscous dissipation. In an effort to further increase the fidelity and complexity of simulated physical phenomena relevant to ICF, the simulations of [8] have now been extended to account for two-component fluids. Results from these new computations are detailed in this paper. This work was motivated by the future need to explore the effect of complex viscosity models for dense plasma mixtures and thermonuclear burn present in ICF capsules, for which a multi-component formulation is required.

The paper proceeds with section II, where a description of the governing equations used to simulate the sudden viscous dissipation of a deuterium-tritium fluid mixture is provided. In section III details of the numerical simulation, such as the initialization scheme, are described. The results are shown in section IV, and the paper wraps up with conclusions in section V.

II. Governing Equations

The starting point are the Navier-Stokes equations for a non-reacting multicomponent fluid, which are given below

$$\frac{\partial \rho}{\partial t} + \frac{\partial \rho u_i}{\partial x_i} = 0, \tag{1}$$

$$\frac{\partial \rho u_i}{\partial t} + \frac{\partial \rho u_i u_j}{\partial x_j} = \frac{\partial \sigma_{ij}}{\partial x_j}, \tag{2}$$

$$\frac{\partial \rho E}{\partial t} + \frac{\partial \rho E u_i}{\partial x_i} = \frac{\partial u_i \sigma_{ij}}{\partial x_j} - \frac{\partial q_i}{\partial x_i}, \tag{3}$$

$$\frac{\partial \rho Y_\alpha}{\partial t} + \frac{\partial \rho Y_\alpha u_i}{\partial x_i} = -\frac{\partial J_{\alpha,i}}{\partial x_i}. \tag{4}$$

In the above, ρ is the density, u_i the velocity, σ_{ij} the stress tensor, E the total energy, q_i the heat flux, Y_α the mass fraction for species α, and $J_{\alpha,i}$ the diffusive species flux.

The velocity field can be decomposed into Favre-averaged and Favre-fluctuating velocities $\widetilde{u}_i$ and u_i'', respectively, so that $u_i = \widetilde{u}_i + u_i''$. As done in [3], the compression of the turbulent flow is achieved by enforcing a predetermined mean flow of the form $\widetilde{u}_i = G_{ij} x_j$, where the deformation tensor G_{ij} is given by

$$G_{ij} = \frac{\dot{L}}{L} \delta_{ij}. \tag{5}$$

In the above, L is the time-dependent characteristic length of the domain that gets compressed, and $\dot{L}$ is the constant rate of change of L.

As stated in [8], the direct solution of equations (1), (2), (3), (4) is not pursued and instead a modified set of equations is solved to easily account for the effect of the mean flow compression. From (1), (2), (3), (4), an alternate set of equations are derived for the fluctuating variables, which are then transformed to a reference frame that moves with the mean flow [9]. A rescaling of the equations similar to that in [3] is then used to improve stability. Details of this derivation for the case of single-species compressible turbulence are provided in [8]. For the work detailed in this paper, the derivation has been extended to account for the mass-fraction transport equation. The overall set of governing equations solved are thus

$$\frac{\partial \rho}{\partial t} + \frac{\partial \rho u_i''}{\partial x_i} = f^{(\rho)}, \tag{6}$$

$$\frac{\partial \rho u_i''}{\partial t} + \frac{\partial \rho u_i'' u_j''}{\partial x_j} = \frac{\partial \phi_{ij}}{\partial x_j} + f_i^{(u)}, \tag{7}$$

$$\frac{\partial \rho E_t}{\partial t} + \frac{\partial \rho E_t u_i''}{\partial x_i} = \frac{\partial u_i'' \phi_{ij}}{\partial x_j} + \frac{\partial q_i}{\partial x_i} + f^{(e)}, \tag{8}$$

$$\frac{\partial \rho Y_\alpha}{\partial t} + \frac{\partial \rho Y_\alpha u_i''}{\partial x_i} = -\frac{\partial J_{\alpha,i}}{\partial x_i} + f^{(y)}. \tag{9}$$

The viscous, conductive, and diffusive fluxes are

$$\phi_{ij} = -p\delta_{ij} + 2\mu \left[\frac{1}{2} \left(\frac{\partial u_i''}{\partial x_j} + \frac{\partial u_j''}{\partial x_i} \right) - \frac{1}{3} \frac{\partial u_k''}{\partial x_k} \delta_{ij} \right], \tag{10}$$

$$q_i = -\kappa \frac{\partial T}{\partial x_i}, \tag{11}$$

$$J_{\alpha,i} = -\rho \left(D_\alpha \frac{\partial Y_\alpha}{\partial x_i} - Y_\alpha \sum_\beta D_\beta \frac{\partial Y_\beta}{\partial x_i} \right). \tag{12}$$

For the above, p is the pressure, T the temperature, $E_t = e + K_t$ the total energy, $e = C_v T$ the internal energy, $K_t = \frac{1}{2} u_i'' u_i''$ the kinetic energy of the fluctuations, and C_v the specific heat at constant volume. The viscosity, thermal conductivity, and species diffusivity are given by $\mu = \mu_0 (T/T_0)^n$, $\kappa = \mu C_p / Pr$, and $D_\alpha = \mu / \rho Sc_\alpha$, where μ_0 and T_0 represent a reference viscosity and temperature, $n = 5/2$ is the power-law exponent, C_p the specific heat at constant pressure, Pr the Prandtl number, and Sc_α the Schmidt number for species α. Each species behaves as an ideal gas, and thus $p = \rho R T$ is used, where $R = R_u / M_{avg}$ is the ideal gas constant, $R_u = 8.314472 \times 10^7$ [g-cm^2 / mol-s^2-K] the universal gas constant, and M_{avg} the average molar mass. The forcing functions that account for the compressive effect of the mean flow are $f^{(\rho)} = -2\rho \dot{L}$, $f_i^{(u)} = -3\rho u_i'' \dot{L}$, $f^{(e)} = -\left[2\rho E_t + \rho u_i'' u_i'' + 3P\right] \dot{L}$, and $f^{(y)} = -2\rho Y_\alpha \dot{L}$.

III. Numerical Details

Equations (6), (7), (8), and (9) are solved using the high-order code Miranda. Spatial derivatives are discretized using a tenth-order Padé scheme, whereas temporal integration is performed with a fourth-order five-stage Runge-Kutta integrator. The Miranda solver employs an artificial fluid approach, for which artificial transport terms are added to the bulk viscosity, thermal conductivity, and molecular diffusivity [10, 11].

The computational domain is a box with 128^3 evenly-spaced grid points. Periodic boundary conditions are applied to the six faces of the domain. Only two mass fractions are present in the system, namely that of deuterium Y_D and tritium Y_T. The molar masses used for deuterium and tritium are 2.01355 [g/mol] and 3.0155 [g/mol], respectively. The ratio of specific heats is $\gamma = 5/3$ and the Prandtl number is $Pr = 1$. The Schmidt number for deuterium is $Sc_D = 0.1$, and that for tritium is $Sc_T = 10.0$.

The initial flow field was extracted from a simulation of forced compressible turbulence [12, 13]. Whereas the linear functions of [12] are used to separately force the solenoidal and dilatational components of velocity so as to achieve target solenoidal and dilatational dissipations, an additional linear forcing function is used in the mass-fraction transport equation to achieve predetermined values of mass-fraction-variance dissipation. The temporal evolutions of the TKE $k = \frac{1}{2} \widetilde{u_i'' u_i''}$ and mass-fraction variance $V = \widetilde{Y_D'' Y_D''} = \widetilde{Y_T'' Y_T''}$ are both shown in figure 1. The flow field at the last available time from the linearly-forced simulation is used to initialize the subsequent computations that focus on the effects of the mean-flow compression.

IV. Results

Figure 2 shows the evolution of the TKE as the domain is compressed, and compares these time histories for different compression speeds. The various compression speeds are denoted by the different values of the initial shear parameter $S_0^* = S_0 k_0 / \epsilon_0$, where $S_0 = \dot{L}_0 / L_0$. These results are also compared against rapid distortion theory [14], which provides exact analytical predictions for infinitely rapid deformations. As the figure shows, the compression of a two-species fluid with a plasma-like viscosity still leads to the sudden viscous dissipation originally demonstrated in [3].

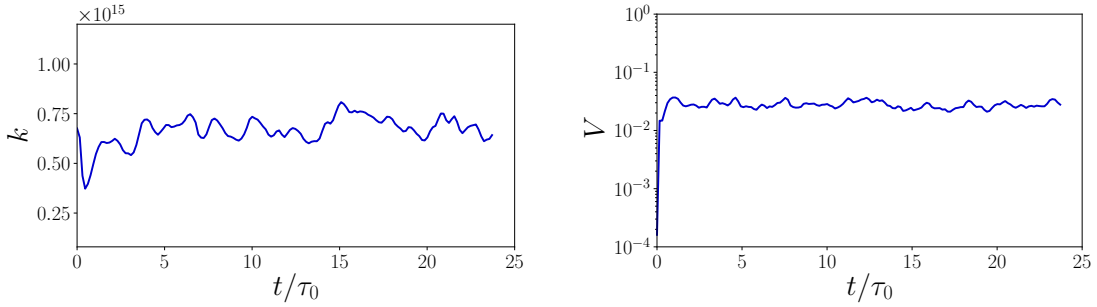

(a) *Turbulent kinetic energy* **(b)** *Mass-fraction variance*

Figure 1: *Time history of TKE and mass-fraction variance for linearly-forced compressible turbulence.*

This TKE evolution is qualitatively similar to cases belonging to both turbulence in the zero-Mach limit [3] and turbulence in the finite-Mach regime [8].

The evolution of $V = \widetilde{Y_D''Y_D''} = \widetilde{Y_T''Y_T''}$ as the compression takes place is shown in figure 3. Unlike for the TKE evolution, the production of mass-fraction variance

$$\overline{\rho}P_\alpha^{(V)} = 2\overline{\rho}\widetilde{Y_\alpha''u_i''}\frac{\partial\widetilde{Y}_\alpha}{\partial x_i} \tag{13}$$

is equal to zero due to the assumption of uniform $\widetilde{Y}_\alpha$, and the only relevant mechanism is that of viscous dissipation, which is given by

$$\overline{\rho}\epsilon_\alpha^{(V)} = 2\overline{\rho D_\alpha \frac{\partial Y_\alpha''}{\partial x_i}\frac{\partial Y_\alpha''}{\partial x_i}}. \tag{14}$$

Thus, V can only remain constant or decay. For the slowest compression rate $S^* = 0.5$, an exponential decay occurs immediately following the start of the compression, whereas, for the fastest compression speed, the mass-fraction variance decays little throughout the initial phase of the compression. Nonetheless, once L has reached sufficiently small values, all simulations show that the flow has fully re-laminarized, both in terms of velocity and mass-fraction fluctuations. We also note that if the evolution of V is shown in a log-scale, as done for the TKE in figure 2, then the decay of the variance appears sudden and rapid.

V. Conclusions

Simulations of the sudden viscous dissipation have been extended to account for the presence of two species, namely deuterium and tritium. It has been shown that the sudden viscous dissipation of TKE still occurs for this two-component fluid. However, more relevant to the current study is that the simulations demonstrate that the mass-fraction variances dissipate as the compression proceeds, and that this decay occurs at markedly different rates for the different compression speeds. The decay of the mass-fraction variance is quite rapid if visualized on a log scale, as is the case for the sudden viscous dissipation of TKE.

This work paves the way for further studies that increase the fidelity and complexity of simulations of the sudden viscous dissipation relevant to ICF. Future efforts are to conduct simulations with a larger number of components with material properties that differ significantly

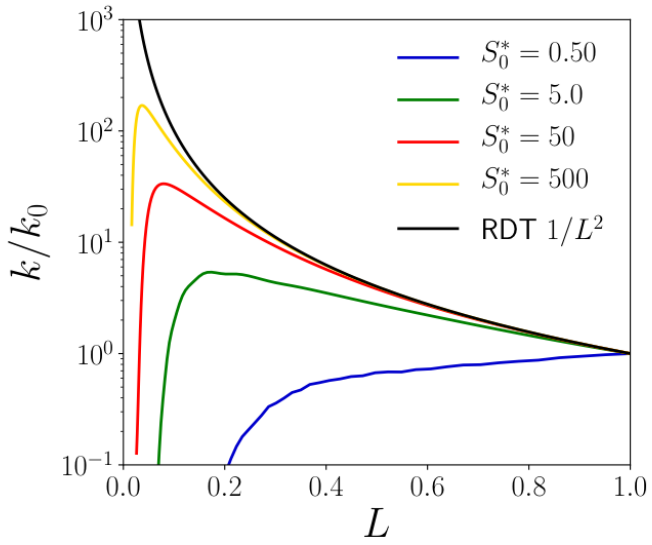

Figure 2: *Evolution of the turbulent kinetic energy k, normalized by its initial value k_0, as the size L of the domain is decreased. The various lines correspond to different values of the initial shear parameter $S_0^* = S_0 k_0/\epsilon_0$, where $S_0 = \dot{L}_0/L_0$.*

from each other. This would then allow for a rigorous testing of complex viscosity models for multi-component mixtures, as well as the study of effects of nuclear reactions on the internal energy of the system.

VI. Acknowledgements

This work was perfomred under the auspices of the U.S. Department of Energy by Lawrence Livermore National Laboratory under Contract DE-AC52-07NA27344.

References

[1] K. A. Flippo et al. (2018). Late-time mixing and turbulent behavior in high-energy-density shear experiments at high Atwood numbers. *Phys. Plasmas*, 25(056315).

[2] P. Wang (2018). Three-dimensional design simulations of a high-energy density reshock experiment at the National Ignition Facility. *ASME J. Fluids Eng.* Vol. 140, pp. 041207.

[3] S. Davidovits and N. J. Fisch (2016). Sudden viscous dissipation of compressing turbulence. *Phys. Rev. Lett.*, 116(105004).

[4] S. Davidovits and N. J. Fisch (2016). Compressing turbulence and sudden viscous dissipation with compression-dependent ionization state. *Phys. Rev. E* 94(053206).

[5] S. Davidovits and N. J. Fisch (2017). Modeling turbulent energy behavior and sudden viscous dissipation in compressing plasma turbulence. *Phys. Plasmas* 24(122311).

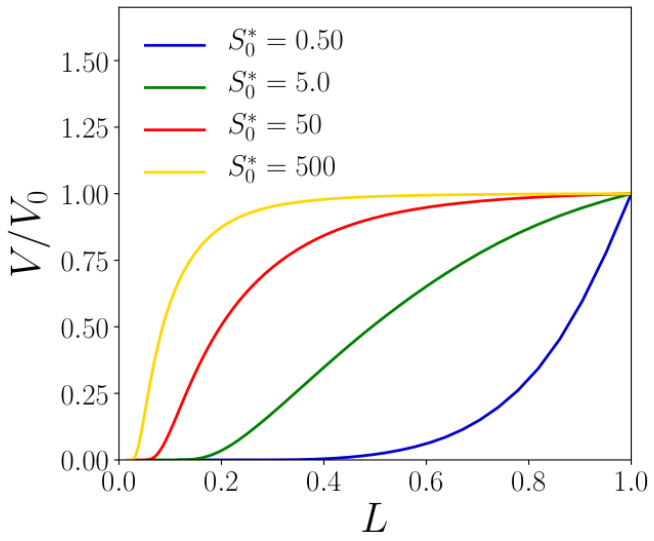

Figure 3: *Evolution of the scalar variance V, normalized by its initial value V_0, as the size L of the domain is decreased. The various lines correspond to different values of the initial shear parameter $S_0^* = S_0 k_0/\epsilon_0$, where $S_0 = \dot{L}_0/L_0$.*

[6] G. Viciconte, B.-J. Gréa, and F. S. Godeferd (2018). Self-similar regimes of turbulence in weakly coupled plasmas under compression. *Phys. Rev. E* 97(023201).

[7] S. Davidovits and N. J. Fisch (2018). Bulk hydrodynamic stability and turbulent saturation in compressing hot spots. *Phys. Plasmas* 25(042703).

[8] A. Campos and B. Morgan (2018). Self-consistent feedback mechanism for the sudden viscous dissipation of finite-Mach-number compressing turbulence. *Under Review*.

[9] R. S. Rogallo (1981). Numerical experiments in homogeneous turbulence. *Technical Memorandum*, 81315, National Aeronautics and Space Administration.

[10] A. W. Cook (2007). Artificial fluid properties for large-eddy simulation of compressible turbulent mixing. *Phys. Fluids*, 19(055103).

[11] A. W. Cook (2009). Enthalpy diffusion in multicomponent flows. *Phys. Fluids*, 21(055109).

[12] M. R. Petersen and D. Livescu (2010). Forcing for statistically stationary compressible isotropic turbulence. *Phys. Fluids*, 22(116101).

[13] A. Campos and B. Morgan (2018). The effect of artificial bulk viscosity in simulations of forced compressible turbulence. *J. Comp. Physics*, Vol. 371, pp. 111–121.

[14] G. A. Blaisdell, G. N. Coleman, and N. N. Mansour (1996). Rapid distortion theory for compressible homogeneous turbulence under isotropic mean strain. *Phys. Fluids*, 8(10).